*Exploration Geophysics (2005) **36**, 41–49*
Butsuri-Tansa (Vol. 58, No.1)
Mulli-Tamsa (Vol. 8, No.1)

Random heterogeneous model with bimodal velocity distribution for Methane Hydrate exploration

Rie Kamei[1] Masami Hato[2] Toshifumi Matsuoka[1]

Key Words: methane hydrate, bimodal distribution, random heterogeneous, autocorrelation, BSR

ABSTRACT

We have developed a random heterogeneous velocity model with bimodal distribution in methane hydrate-bearing zones. The P-wave well-log data have a von Karman type autocorrelation function and non-Gaussian distribution. The velocity histogram has two peaks separated by several hundred metres per second. A random heterogeneous medium with bimodal distribution is generated by mapping of a medium with a Gaussian probability distribution, yielded by the normal spectral-based generation method. By using an ellipsoidal autocorrelation function, the random medium also incorporates anisotropy of autocorrelation lengths. A simulated P-wave velocity log reproduces well the features of the field data.

This model is applied to two simulations of elastic wave propagation. Synthetic reflection sections with source signals in two different frequency bands imply that the velocity fluctuation of the random model with bimodal distribution causes the frequency dependence of the Bottom Simulating Reflector (BSR) by affecting wave field scattering. A synthetic cross-well section suggests that the strong attenuation observed in field data might be caused by the extrinsic attenuation in scattering.

We conclude that random heterogeneity with bimodal distribution is a key issue in modelling hydrate-bearing zones, and that it can explain the frequency dependence and scattering observed in seismic sections in such areas.

INTRODUCTION

Methane hydrate consists of methane and water molecules that form a cage-like structure. Because hydrate is stable under conditions of low temperature and high pressure, it has been found in sediments under the deep ocean, along continental slopes, and in permafrost regions. Neither the geological nor the seismic model of the gas-hydrate zone is yet fully understood (Collet, 2002), and precise delineation of the hydrate-bearing zone is required in order to explore for and develop methane hydrate as a future energy resource. We develop a velocity model for the hydrate zone as a first step.

[1] *Department of Civil and Earth Resources Engineering Graduate School of Engineering, Kyoto University, Yoshida-hon-cho, Sakyo-ku, Kyoto, Kyoto-fu, Japan, 606-8501*
Phone: +81-75-753-5406
Facsimile: +81-75-753-4775
Email: kamei@earth.kumst.kyoto-u.ac.jp

[2] *JGI Inc. Meikei Bldg, 1-5-21, Otsuka, Bunkyo-ku, Tokyo Japan, 112-0012*

Manuscript received August 9, 2004; accepted November 18, 2004. Part of this paper was presented at the 7th SEGJ International Symposium (2004).

The actual P-wave velocity in hydrate-bearing sediments is not uniformly high across the gas-hydrate stability zone as found in laboratory measurements (e.g., 3.25 km/s: Sloan, 1990) but velocity logs frequently show short-wavelength perturbations compared with non hydrate-bearing sediments (Akihisa et al., 2002). This suggests that the hydrate-bearing zone contains strong vertical heterogeneities, assuming that the high and low velocity intervals correspond to hydrate-rich and hydrate-poor zones respectively.

Reflection seismic surveying is the most effective method for exploration in hydrate-bearing areas, and this method has been extensively employed both with air-gun sources and with the Deep Towed Acoustic/Geophysics System (DTAGS) (Chapman et al., 2002; Ward et al., 2004). For production monitoring, cross-well tomography was experimentally conducted in the Mallik field, Mackenzie Delta, Canada (Watanabe et al., 2004). Seismic profiles acquired in hydrate-bearing areas have displayed some interesting phenomena that have not completely explained. Firstly, the Bottom Simulating Reflector (BSR), the most important indicator of hydrate occurrence, is not always clearly visible in reflection profiles acquired using the DTAGS, which has a source operating in a high-frequency band (250–650 Hz) (Fink and Spence, 1999; Chapman et al., 2002). Secondly, strong wave attenuation was observed in cross-well seismic tomography acquired in the Mallik field (Watanabe et al., 2004). A rough sea floor (Fink and Spence, 1999) or a gradual velocity contrast at the BSR (Chapman et al., 2002) have been proposed as reasons for the weak BSR in DTAGS data. Guerin and Goldberg (2002), in an analysis of Mallik 2L-38 well data, found that a low Q in the methane hydrate zone could be caused by intrinsic attenuation. However, observing that velocity fluctuates quite rapidly in well-logging data, it also becomes necessary to study the effects of scattering in hydrate-bearing zones. Studies of randomly heterogeneous media have shown that short-wavelength (small-scale) heterogeneities scatter the seismic waveform, and consideration of both horizontal and vertical heterogeneities is required (Aki and Richards, 1980; Sato and Fehler, 1997; Levander et al., 1994).

A random medium is mathematically characterised using two functions, the autocorrelation function (ACF), and the probability distribution function (PDF). The ACF describes the configuration of the random medium and is parameterised by the correlation length, which determines the randomness of the medium. The ACF is typically described using well-known analytical forms such as Gaussian, exponential, or von Karman (or self-similar) type autocorrelation functions (Frankel and Clayton, 1986; Wu and Aki, 1985). The ACF cannot fully describe the random medium, except for the Gaussian distribution (Shinozuka and Deodatis, 1996), but requires a PDF. In the case of Gaussian distribution, the spectral-based method is usually adopted for generating random media in seismic studies (Frankel and Clayton, 1986; Kawahara, 1996). For media with non-Gaussian probability distributions, a mapping technique must be exploited (Goff et al., 1994; Yamazaki and Shinozuka, 1988).

In this paper, we developed a 2D short-wavelength randomly heterogenous model for hydrate-bearing zones, based on the

statistical characteristics of P-wave velocity logs, such as their ACF and PDF. Anisotropy of heterogeneities is also introduced to represent lateral continuity in the bedding directions. The model is applied to two simulations of elastic wave propagation, in which synthetic reflection survey profiles and synthetic cross-well profiles are created.

WELL LOG DATA

The data we used in this research were acquired in the Ministry of International Trade and Industry (MITI) Nankai Trough Post Survey Well #1. The MITI data, with trend removed and incorrect values modified, are shown in Figure 1(a). The interval shown consists of thinly bedded sandstone and shale layers, and is rich in hydrate. No massive high-velocity zone can be recognized in the well data, but high-velocity peaks are observed at depths of about 1182, 1206, and 1211 m which may correspond to the hydrate-rich sandstone.

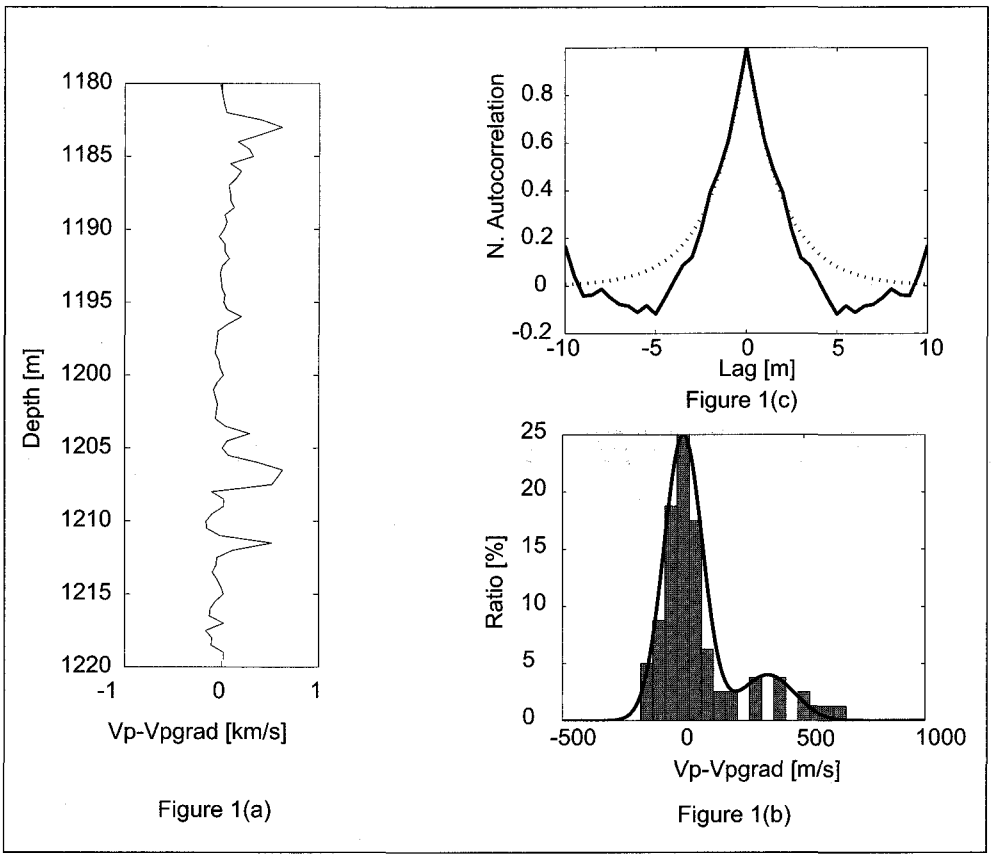

Fig. 1. (a) P-wave velocity log of MITI Nankai Trough Post Survey Well #1 after velocity gradient has been removed. The solid line in (b) is the ACF of the real well log data and a dashed line is the best-matching ACF. (c) displays the histogram and the solid line is the best-fit PDF.

The characteristic functions for random media, the ACF and the PDF of the P-wave data, are estimated from the well-log data. The ACF of the MITI data, shown in Figure 1(b), is best modelled with a von Karman (vK) type ACF:

$$N(r)=\frac{2^{1-\nu}}{\Gamma(\nu)}\left(\frac{r}{a}\right)^{\nu}K_{\nu}\left(\frac{r}{a}\right), \qquad (1)$$

where $r = |\mathbf{r}|$, $\mathbf{r}$ is a distance vector, a is the autocorrelation length, ν is the Hurst number, Γ is the Gamma function, and K_ν is the modified Bessel function of the second kind and order ν. The vK type is known to represent well the characteristics of the Earth's interior (Kawahara, 1997)

The histogram of the velocity log, shown in Figure 1(c), has two peaks at around 0 m/s and 350 m/s, and the histogram in the vicinity of each peak is quite similar to a Gaussian distribution. The high-velocity peak corresponds to two peaks in Figure 1(a). Therefore the PDF describing velocity structure of these hydrate-bearing sediments becomes the superposition of two Gaussian distributions:

$$h(c_b)=\sum_{i=1}^{2} w_i \frac{1}{\sqrt{2\pi}\,\sigma_i}\exp\left[-\frac{(c_b-\mu_i)^2}{2\sigma_i^2}\right], \qquad (2)$$

and called a "bimodal distribution" in this paper. The bimodal PDF is $h(c_b)$, where c_b is the velocity, and w_i, μ_i, and σ_i are the ratio, mean value and standard deviation of the ith contribution. Hereafter, suffix 1 and 2 refers to the high- and low-velocity contributions, respectively. Parameters best fitted to the log data are $w_1 = 0.18$, $\mu_1 = 350$, $\sigma_1 = 80$, $w_2 = 0.82$, $\mu_2 = 0$ and $\sigma_2 = 30$ m/s. Our model of hydrate-bearing zones is of sediments composed of high velocity (hydrate-rich) and low velocity (little or no hydrate) parts, to give this velocity probabiltiy distribution.

MODELLING METHODOLOGY

We adopt a spectral-based approach to develop a randomly heterogeneous model for the hydrate-bearing zone, using the vK-type ACF and the bimodal PDF discussed above. The method for generating 1D, 2D, and 3D randomly heterogeneous media having a Gaussian distribution of components is well developed (Kawahara, 1996; Shinozuka, 1996). A randomly heterogeneous medium with a non-Gaussian distribution can be derived from a reference medium with a Gaussian distribution by using a cumulative probability distribution function (Goff et al., 1994; Yamazaki and Shinozuka, 1988). Since this conversion is non-linear, the ACF of the resulting bimodal random medium may not agree with the ACF desired. To overcome this problem, Yamazaki and Shinozuka (1988) proposed an iterative procedure, and we adopt this approach to match the ACFs here.

Random medium with Gaussian distribution

First, we review the method to generate a 2D Gaussian random velocity field with Gaussian distribution, $c_g(\mathbf{x})$, with a mean value μ and a standard deviation σ. The medium's ACF $N(\mathbf{r})$ is defined as

$$N(\mathbf{r})=\frac{E\left[c_g(\mathbf{x})+r-\mu\right]E\left[c_g(\mathbf{x})-\mu\right]}{\sigma^2}, \qquad (3)$$

where **r** is a separation distance vector. $N(\mathbf{r})$ is related to the power spectrum density function (PSDF) of the medium, $H_g(\mathbf{K})$, by the Wiener-Khintchine theorem

$$H_g(\mathbf{K}) = F[N(\mathbf{r})], \quad (4)$$

where **K** is the wave number vector and F denotes a 2D Fourier Transform. $H_g(\mathbf{K})$ is often defined analytically, and $H_g(\mathbf{K})$ for a 2D vK-type ACF becomes

$$S_g(\mathbf{K}) = \frac{2\nu a^2}{\left(1+K^2a^2\right)^{\nu+1}}, \quad (5)$$

with $K = |\mathbf{K}|$. Therefore, a reference medium $c_{g0}(\mathbf{x})$, with zero mean and unit standard deviation, can be generated using the 2D Inverse Fourier Transform

$$c_{g0}(\mathbf{x}) = F^{-1}\left[\sqrt{S_g(\mathbf{K})}\, e^{iK\theta}\right], \quad (6)$$

where θ is the phase angle, set to be uniformly random. Note that the probability distribution of the resulting random medium, $c_g(\mathbf{x})$, is asymptotically Gaussian because of the central limit theorem (Shinozuka and Deodatis, 1991). Then, the velocity field with mean value μ and standard deviation σ is,

$$c_g(\mathbf{x}) = \sigma c_{g0}(\mathbf{x}) + \mu. \quad (7)$$

To generate a 1D random medium, all vectors in the above equations are replaced by scalars and a 1D Fourier Transform is used instead of a 2D transform.

Random medium with bimodal distribution

The random medium with bimodal distribution can be mapped from the Gaussian random medium (Goff et al., 1994, Yamazaki and Shinozuka, 1988). The mapping formula is

$$H_b[c_b(\mathbf{x})] = H_g[c_{g0}(\mathbf{x})], \quad (8)$$

where H_g and H_b are the cumulative PDFs of Gaussian and bimodal distributions and are described by

$$H_g[c_{g0}(\mathbf{x})] = \frac{1}{2}\left[1+\mathrm{erf}\left(\frac{c_{g0}(\mathbf{x})}{\sqrt{2}}\right)\right], \text{ and} \quad (9)$$

$$H_b[c_b(\mathbf{x})] = \frac{1}{2}\left[1+\sum_i \mathrm{erf}\left(\frac{c_b(\mathbf{x})-\mu_i}{\sigma_i\sqrt{2}}\right)\right], \quad (10)$$

where erf denotes the error function. By substituting equation (9) and equation (10) into equation (8), and finding the root of equation (8), $c_b(\mathbf{x})$ can be calculated. Unfortunately, this mapping is non-linear and the ACF and PSDF of the resulting bimodal random medium do not coincide with the desired distribution. Yamazaki and Shinozuka (1988) proposed to modify an input PSDF, $S_g(\mathbf{K})$, iteratively to match the desired PSDF, S_d. We use their method to determine the input $S_g(\mathbf{K})$, with details described in the Appendix. In summary, the procedure to generate the bimodal PDF of a random medium is as follows:

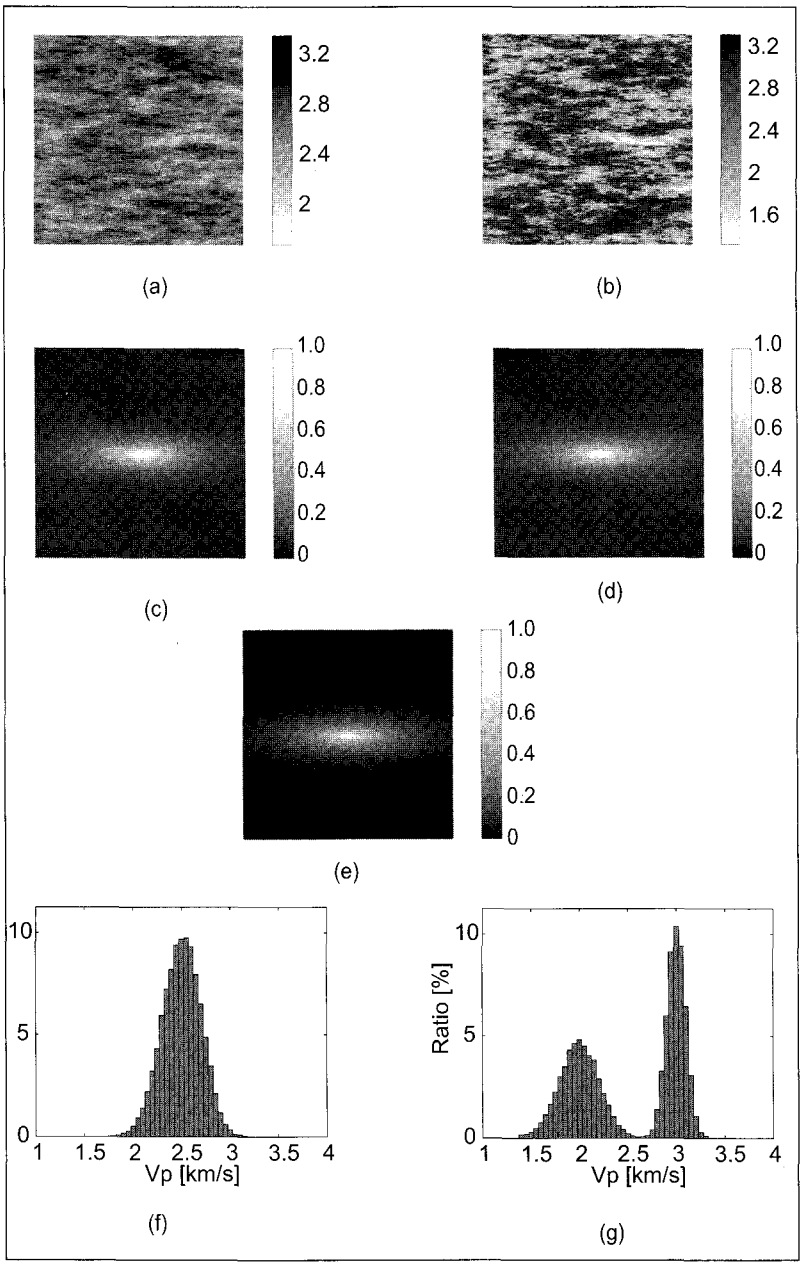

Fig. 2. An example of 2D anisotropic randomly heterogeneous media, 200 × 200 m width. The left column ((a), (c), and (e)) is a medium with Gaussian probability distribution, with μ = 2500 m/s and σ = 200 m/s, and the right column ((b), (d), and (f)) is a medium with bimodal probability distribution with w_1 = 0.50, μ_1 = 3 000 m/s, σ_1 = 300 m/s, μ_2 = 2 000 m/s and σ_2 = 200 m/s. From top to bottom, the figures are: the medium with velocities represented by grey levels ((a), (b)), velocity histograms ((c), (d)) and ACF ((e), (f)). (g) is a desired ACF.

1. Estimate the ACF and PDF of the component media from P-wave logs.
2. Estimate the power spectrum density function (PSDF) of a reference random medium with Gaussian distribution, $S_g(\mathbf{K})$.
3. Generate a reference random medium with a Gaussian distribution, $c_{g0}(\mathbf{x})$.
4. Map to the desired random medium with a bimodal distribution, $c_b(\mathbf{x})$.

Introduction of anisotropy

In 2D geological structures, the autocorrelation function (ACF) is usually not a symmetric function because of anisotropy introduced by the sedimentation process. Therefore, the correlation length

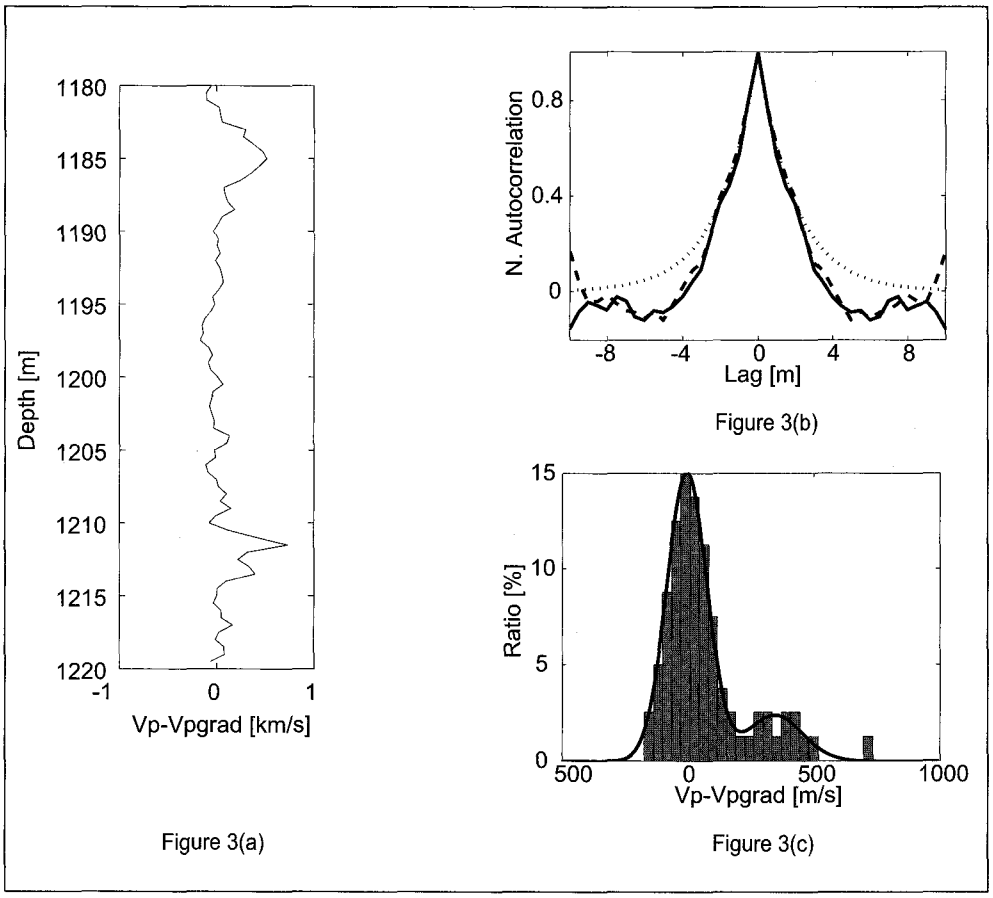

Fig. 3. (a) Simulated well log for Nankai Trough Post Survey Well #1. (b) Solid line is the ACF of observed well log data, dotted line is an estimated ACF, and dashed line is that for the simulated log. (c) Histogram of real well log data; solid line is the estimated PDF.

vector $\mathbf{a} = (a_x, a_z)$ varies with direction, $\tan^{-1}(a_z/a_x)$. In many field data examples, the horizontal correlation length is longer and the vertical one shorter because of sedimentation anisotropy. Ikelle et al. (1993) proposed the ellipsoidal correlation function,

$$r/a = \sqrt{(r_x/a)^2 + (r_z/b)^2}\ , \qquad (11)$$

$$Ka = \sqrt{(K_x a)^2 + (K_z b)^2}\ , \qquad (12)$$

where a and b are the correlation lengths in the horizontal and vertical Cartesian directions. The aspect ratio $r_0 = b/a$ is sometimes useful to characterise the shape of anisotropy. In the case of isotropic media, $a = b = 1$ and r_0 is unity, and in the case of a vertically stratified random medium, r_0 is zero. When the direction of longest correlation length is not horizontal, generation of velocity functions for the medium requires rotating the Cartesian coordinate axes and setting a new x direction appropriately.

Example

Examples of anisotropic random media with Gaussian and bimodal distributions, and with aspect ratio 0.25, are shown in Figure 2. Lateral anisotropy is visible in both media (Figures 2(a) and 2(b)) and both ACFs are ellipsoidal (Figures 2(c) and 2(d)), and match well with the desired ACF in Figure 2(e). The velocity in the Gaussian medium is distributed around 2.5 km/s (Figure 2(f)) and that in the bimodal medium is distributed around 3 km/s and 2 km/s (Figure 2(g)). Our method can generate a random medium that is able to replicate both ACFs and probability distributions.

EVALUTION OF THE RANDOM MODEL WITH BIMODAL DISTRIBUTION

We evaluate our generation methodology by comparing a simulated P-wave velocity log with the log from the Nankai Trough (Figure 1(a)). A simulated P-wave velocity log, i.e., a 1D random model with bimodal velocity probability distribution is created, using the parameters estimated in the Well-Log Data section above, and is shown in Figure 3(a). The simulated log has high-

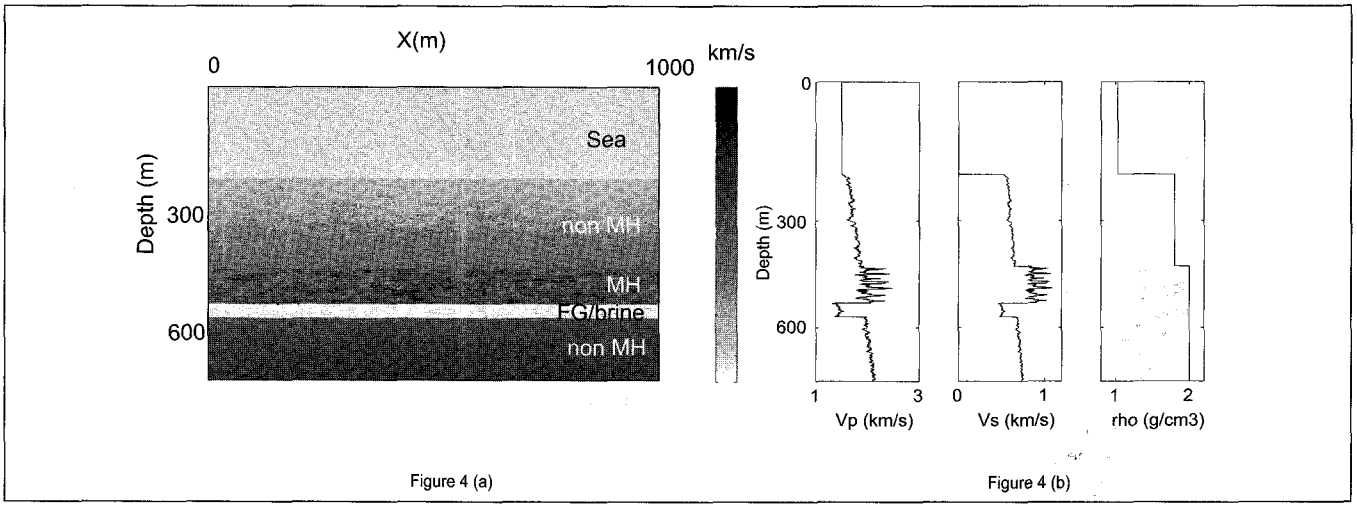

Fig. 4. The velocity structure for Simulation 1. (a) P-wave velocity structure. (b) from left to right, P-wave velocity, S-wave velocity, and density log at x = 500 m.

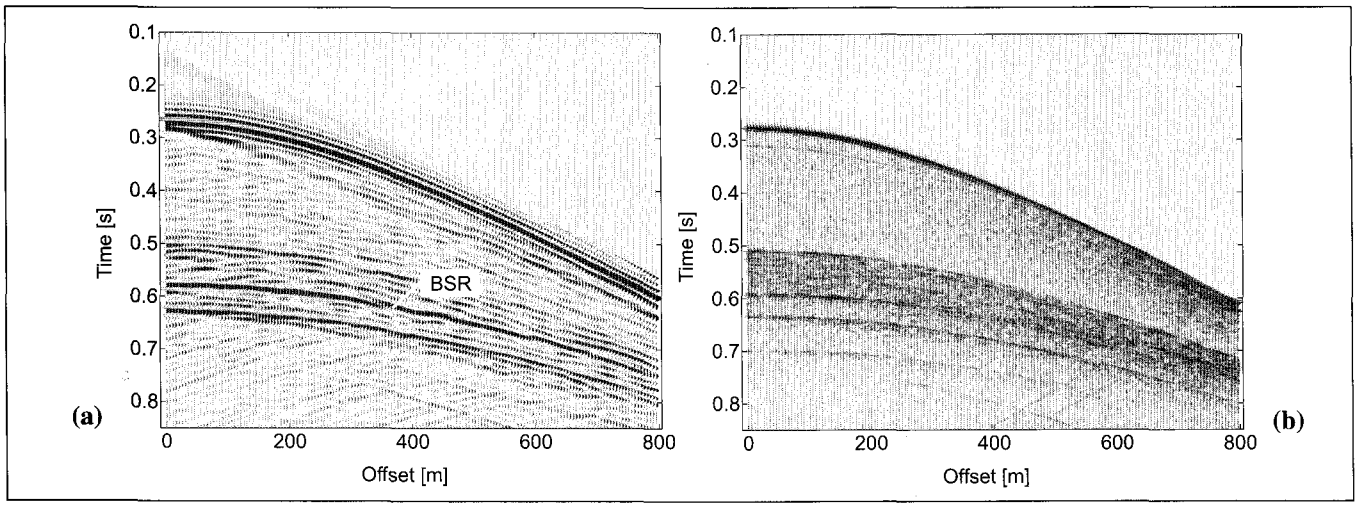

Fig. 5. Shot gathers from Simulation 1 (reverse polarities). (a) 4–80 Hz source signal (airgun) and (b) 250–650 Hz source signal (DTAGS).

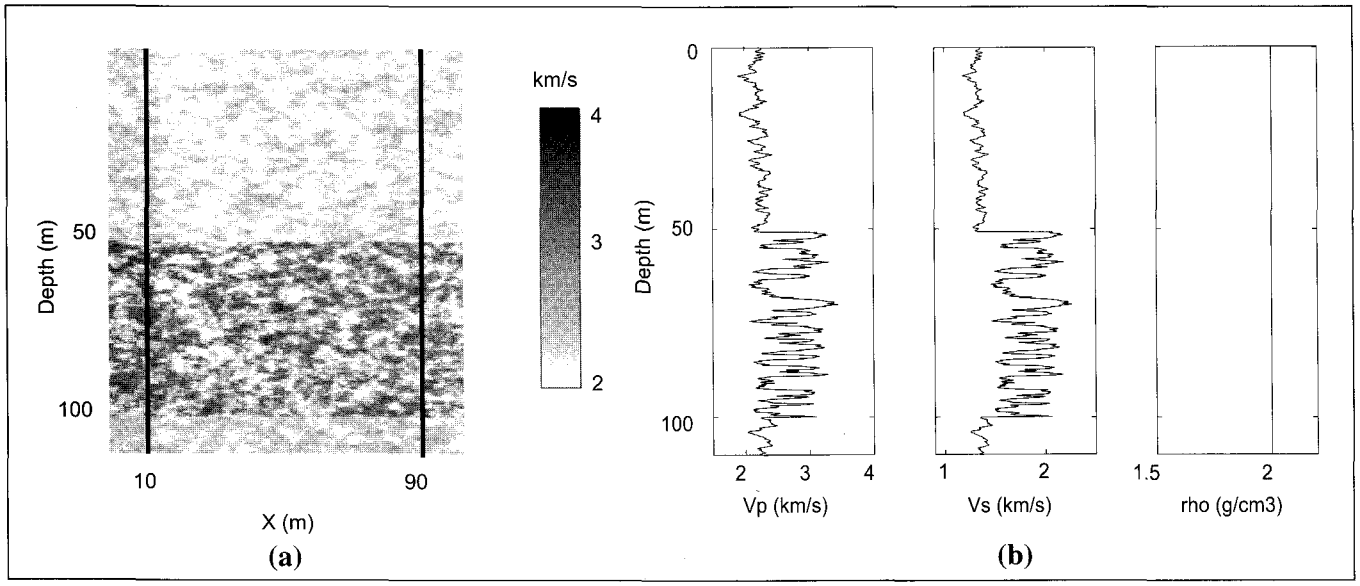

Fig. 6. The velocity structure for Simulation 2. (a) P-wave velocity structure. Vertical lines at x = 10, 90 m indicate well locations. Sources and receivers are located in the left and right wells, respectively. (b) from left to right, P-wave velocity, S-wave velocity and density log at x = 45 m.

velocity peaks at about 1185 and 1210 m and a small-scale velocity fluctuation. These features are also found in the real log (Figure 1(a)). The ACF and PDF of the simulated and real logs agree fairly well (compare Figures 1(b), (c) with Figures 3 (b), (c)). This test confirms that our methodology has the ability to demonstrate the features of real logs.

APPLICATION

The random model with bimodal distribution is applied to the simulation of elastic wave propagation and the resulting seismic profiles are examined. The adopted simulation algorithm is a staggered grid finite difference method with the elastic wave equation (Virieux 1986; Levander, 1988).

Simulation 1: Reflection survey

In reflection surveys over hydrate-bearing areas, DTAGS has been used to acquire high-resolution data to complement the data obtained with air-gun sources. In this simulation, two frequency source bands, 4–80 Hz (corresponding to the ordinary air gun source) and 250–650 Hz (corresponding to DTAGS), are used to evaluate the difference in their synthetic seismic sections.

Our geological model is based on MITI Nankai Trough data (Akihisa et al., 2002), and comprises five zones, seawater, upper zone (200 m), hydrate-bearing zone (80 m), low-velocity zone containing free gas or brine (30 m), and deeper zone. A random medium with bimodal probability distribution is adopted only in the hydrate-bearing zone, and in the other zones we assume random media with Gaussian distributions. In our velocity model, P- and S-wave velocities are perturbed but density and Poisson's ratio are held constant, as is shown in Table 2. The small-scale parameters for hydrate-bearing zone are set equal to those observed in the Well-Log Data section above. Because the aspect ratio of the autocorrelation function cannot be obtained directly from this well log data, we used a value of 0.25 from the study by Ikelle et al. (1994). The variation in properties with depth is shown in Figure 4.

The simulation results are shown in Figure 5, for a source is located in the water at x = 50 m and 161 receivers are located at the same level, at 2-m intervals, with the nearest offset 100 m. In Figure 5(a), the seismic section with a low frequency source (4–80 Hz), clear reflection events are observed at the interfaces such as the BSR at the base of the hydrate-bearing zone, as expected from the strong impedance contrast. The interface between the upper non-

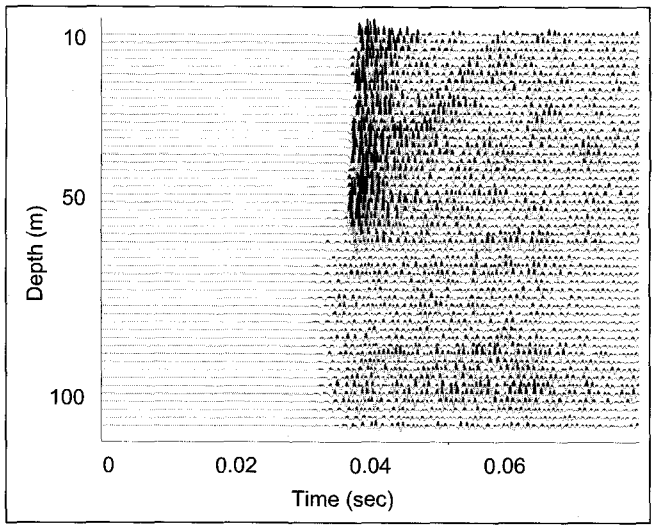

Fig. 7. Synthetic gather, for sources and receivers on the same level, in Simulation 2.

hydrate-bearing zone and the hydrate-bearing zone is indistinct, because the impedance contrast is not laterally continuous. Weak scattered waves can also be seen. The seismic section with a high-frequency source (250–650 Hz) is markedly different from that with the low-frequency source. Reflection events in Figure 5(b) are not clear even at the base of the hydrate-bearing zone, where the BSR is expected, and much more scattering is observed. In the hydrate-bearing zone, the random medium with bimodal property distribution exacerbates the high-frequency scattering and makes the BSR invisible.

Simulation 2: Cross-well survey

In the Mallik field, Canada, cross-well tomography was conducted in 2002 to monitor gas hydrate production (Watanabe et al., 2004). We apply our random model to the cross-well simulation and examine the scattering effects.

In this simulation, our simplified model consists of three horizontal layers, a hydrate-bearing zone bounded by two non-hydrate-bearing zones. As in Simulation 1, the random velocity model with bimodal probabiltiy distribution is adopted only in the hydrate-bearing zone, and Gaussian distribution in the non-hydrate-bearing zones (Table 2). P- and S-wave velocities are perturbed and density and Poisson's ratio are constant, as in Simulation 1. We assumed the aspect ratio of autocorrelation lengths to be 0.5 in this case. The P-wave velocity structure is shown in Figure 6. The distance between wells in which sources and receivers are located were set to be 80 m. A Ricker wavelet with a centre frequency of 1 kHz was used as a source function.

The simulation results are shown in Figure 7, in which a reflection from the top of the hydrate-bearing zone can be seen. The first arrivals in the hydrate-bearing zone are earlier because of the higher velocity, but their amplitudes are weak compared to non-hydrate-bearing zones. The strong velocity variation in the hydrate-bearing zone is considered to cause scattering and reduce the transmitted energy observed in Figure 7.

Discussion of the simulation results

The two simulations suggest that the pattern of small-scale velocity variation considerably affects seismic profiles, but the effect is a function of wavelength (i.e., frequencies). The synthetic seismic profiles reproduce the features in observed seismic sections, which we summarize as:

- When a high-frequency source (such as the DTAGS) is adopted, major reflectors below the hydrate-bearing zone are weakened in comparison with reflections using a low-frequency source (corresponding to the ordinary air gun source).
- The synthetic cross-well logs illustrate the extrinsic attenuation occurring in hydrate-bearing sediments.

The first result supports a hypothesis that short-wavelength heterogeneities can be a major cause of BSR variability. This means that a BSR-like reflector may be difficult to recognize with a high-frequency source. Because the effects of random heterogeneity are known to depend on the autocorrelation lengths a, b, travel distance L, and the wavelength, the magnitudess of non-dimensional numbers ka, kb, and kL are key factors for the analysis (k is the wavenumber). Figure 8 illustrates the classification regime of Aki and Richards (1980). The classification suggests that the relatively small kb of a low-frequency source suppresses the heterogeneities, reducing the random medium to an equivalent homogeneous medium, which results in the clear appearance of the BSR in Figure

Zone	V_{p0} m/s	V_{pinc} m/s/m	ν_p	ρ g/cm^3	ν	r_0	b m	k_hb	k_lb	μ_1 m/s	σ_1 m/s	μ_2 m/s	σ_2 m/s	w_1 %
upper non hydrate-bearing	1610	1.12	0.35	1.8	0.4	0.25	3	0.46	0.7	0	0	-	-	-
hydrate-bearing	1834	1.12	0.25	2.0	0.5	0.25	2	0.27	1.6	350	80	0	30	18
low velocity	1500	0	0.20	2.0	0.25	0.25	2	0.35	2.1	0	40	-	-	-
lower non hydrate-bearing	1968	1.12	0.35	2.0	0.3	0.25	3	0.38	2.3	0	40	-	-	-

Table 1. Elastic and stochastic parameters for Simulation 1: Reflection survey. Elastic parameters V_{p0}, V_{pinc}, υ_p, and ρ are P-wave velocity at the top of each zone, V_p gradient, Poisson's ratio, and density, respectively. Stochastic parameters for the ACF, ν, r_0, and b are Hurst number, aspect ratio, and autocorrelation length. k_hb and k_lb imply the effects on seismic wave where k_h and k_l are mean wavenumbers at the centre frequency of the high- and low-frequency sources, respectively. The other stochastic parameters for the Gaussian or bimodal PDF, μ_i, σ_i, and w_i, are mean velocity, standard deviation, and volume ratio of the ith portion.

Zone	V_{p0} m/s	V_{pinc} m/s/m	ν_p	ρ g/cm^3	ν	r_0	b m	kb	μ_1 m/s	σ_1 m/s	μ_2 m/s	σ_2 m/s	w_1 %
upper non hydrate-bearing	2000	1.0	0.35	1.8	1.0	0.5	0.6	1.8	0	115	-	-	-
hydrate-bearing	2050	1.0	0.25	2.0	1.0	0.5	0.65	1.6	750	200	0	17	58
lower non hydrate-bearing	2100	1.0	0.35	2.0	1.0	0.5	0.6	1.8	0	115	-	-	-

Table 2. Elastic and static parameters for Simulation 2: Cross-well survey. Variables are set as Table 1. In this case, the wavenumber k is that of the centre frequency, 1kHz.

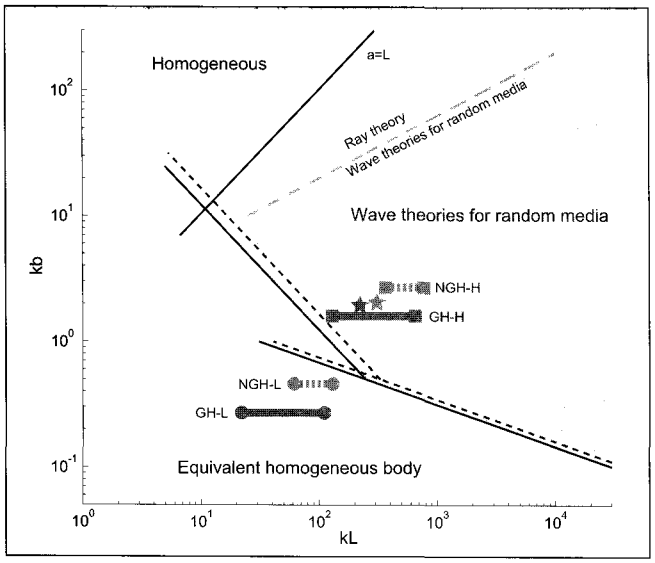

Fig. 8. Classification of scattering problems and applicable methods on a *ka–kL* diagram (modified from Aki and Richards, 1980). NGH-L, NGH-H, GH-L and GH-H refer to possible *ka–kL* ranges for non-hydrate-bearing zone (NGH) and hydrate-bearing zone (GH) with low (-L) and high (-H) frequency sources, respectively. Dark and light stars indicate *ka–kL* points for hydrate-bearing and non-hydrate-bearing zones in the cross-well model (Simulation 2). *L* is a representative wave travel distance in each zone.

5(a). The *kb* value of the high-frequency source is, however, in the range where the random theory should be considered. This would explain why only the high-frequency source wavelet was able to reflect from the small-scale inhomogeneities in the velocity structure, adding to the number of scattered waves.

Figure 8 also shows that the non-hydrate-bearing zone and hydrate-bearing zone points for each source plot close together in the *kb–kL* classification. However, seismic waves from a high-frequency source are scattered much more strongly in the hydrate-bearing zone compared to the upper non-hydrate-bearing zone. This demonstrates the advantages of a bimodal probability distribution over a Gaussian distribution in the hydrate-bearing zone, because it is likely that the use of a Gaussian distribution in the hydrate-bearing zone would probably not generate the BSR variability which is observed. The autocorrelation length aspect ratio also affects the seismic wave in 2D random media (Ikelle et al., 1994) but it is not possible to measure horizontal autocorrelation lengths at this time, and our results are calculated for a fixed aspect ratio in both cases.

The hydrate-bearing zone in the Mallik field is considered to be thick and massive, unlike that in the Nankai Trough in which thinly layered hydrate-rich sandstone alternates with shales. The attenuation observed has been considered to be caused by intrinsic attenuation associated with low Q in the methane hydrate zone (Guerin and Goldberg, 2002). It may be difficult to adopt the results of our short-wavelength velocity model directly to Mallik field conditions. However, our cross-well results suggest that scattering attenuation is also possible and should be considered carefully in cross-well simulations of highly heterogeneous areas such as the hydrate zone in the Nankai Trough.

CONCLUSIONS

In this paper, we have modelled a hydrate-bearing zone as a randomly heterogenous medium and derived two important stochastic features of hydrate-bearing zones. We found that the ACF of hydrate-bearing zones can be represented by a von Karman-type function, and that the velocity probability distribution in hydrate zones is not a Gaussian distribution, but a bimodal distribution, the PDF of which can be described as the superposition of Gaussian PDFs. The bimodal distribution requires modification to the ordinary spectral-base method of generating property distributions in a random medium. We have developed such a method for 2D randomly heterogeneous models for hydrate-bearing zones, in which we iteratively map from a random medium with Gaussian PDF, and our method is able to reproduce the required ACF, PDF, and anisotropy.

The validity and applicability of our hydrate-zone model were evaluated by two numerical simulations, of reflection and cross-well surveys. The reflection survey test successfully demonstrated the possibility that the appearance of the BSR may be frequency-dependent, and the advantage of using a bimodal distribution to predict it. Using a classification in *ka–kL* space will contribute to understanding this. The synthetic cross-well section demonstrates the possibility of scattering attenuation in the heterogeneous hydrate-zone. We conclude that our randomly heterogeneous model with the bimodal distribution has successfully modelled hydrate-bearing zones and has the potential to explain observed features of seismic sections acquired in such areas.

ACKNOWLEDGEMENT

The authors thank Dr. Watanabe of Nagoya University for providing his elastic waveform simulation program.

REFERENCES

Aki, K., and Richards, P.G., 1980, *Quantitative Seismology; Theory and methods, vol. 2*: W.H. Freeman and Co., pp749.

Akihisa, K., Tezuka, K., Senoh, O., and Uchida, T., 2002, Well log evaluation of gas hydrate saturation in the MITI Nankai Trough well, offshore south east Japan: *SPWLA 43rd Annual Logging Symposium, Oiso, Japan*, Paper BB.

Chapman, N.R., Gettrust, J.F., Walia, R., Hannay, D., Spence, G.D., Wood, W.T., and Hyndman, R.D., 2002, High-resolution, deep-towed, multi channel seismic survey of deep sea gas hydrates off western Canada: *Geophysics*, **67**, 1038–1047.

Collet, T.S., 2002, Energy resource potential of natural gas hydrates: *AAPG Bulletin*, **86**, 1971–1992.

Goff, J.A., Holliger, K., and Levander A.R., 1994, Modal fields: a new method for characterization of random seismic velocity heterogeneity: *Geophysical Research Letters*, **21**, 493–496.

Guerin, G. and Goldberg, D., 2002, Sonic waveform attenuation in gas hydrate-bearing sediments from the Mallik 2L-38 research well, Mackenzie Delta, Canada: *Journal of Geophysical Research*, **107**(B5), EPM1.

Fink, C., and Spence, G.D., 1999, Hydrate distribution off Vancouver Island from multifrequency single channel seismic reflection data: *Journal of Geophysical Research*, **104**, 2909–2922.

Frankel, A., and Clayton, R.W., 1986, Finite difference simulations of seismic scattering: Implications for the propagation of short-period seismic waves in the crust and models of crustal heterogeneity: *Journal of Geophysical Research*, **91**, 6465–6489.

Ikelle, L.T., and Yung, S.K., 1993, 2D random media with ellipsoidal auto correlation function: *Geophysics*, **58**, 1359–1372.

Kawahara, J., 1997, Numerical Simulations of Seismic Wave propagation in Random Media: *Zishin*, **50**, 135–156.

Levander, A., 1988, Fourth-order finite-difference P-SV seismograms: *Geophysics*, **53**, 1425–1436.

Shinozuka, M., and Deodatis, G., 1991, Simulation of stochastic processes by spectral representation: *Appl. Mech. Rev.*, **44**, 191–204.

Levander, A., Hobbs, R.W., Smith, S., K., England, R.W., Snyder, D.B., and Holliger, K., 1994, The crust as a heterogeneous "optical" medium" or "crocodiles in the mist": *Tectonophysics*, **232**, 281–297.

Sato, H., and Fehler, M.L., 1997, *Seismic Wave Propagation and Scattering in the Heterogeneous Earth*: Springer-Verlag.

Sloan, E.D., 1990, *Clathrate hydrates of natural gases*, Marcel Dekker, pp641.

Virieux, J., 1986, P-SV wave propagation in heterogeneous media: velocity-stress finite-difference method: *Geophysics*, **51**, 889–901.

Ward, P., Asakawa, E., and Shimizu, S., 2004, High Resolution, Deep-Tow Seismic Survey to Investigate the Methane Hydrate Stability Zone in the Nankai Trough: *Resource Geology*, **54**, 115–124.

Watanabe, T., Shimizu, S., Asakawa, E., Kamei, R., and Matsuoka, T., Preliminary assessment of the waveform inversion method for interpretation of cross-well seismic data from the thermal production test, Mallik Gas Hydrate Production Research Well, Scientific Results from Mallik 2002 Gas Hydrate Production Research Well Program, Mackenzie Delta, Northwest Territories, Canada, (ed.) Dallimore, Uchida, and Collett; Geological Survey of Canada, Bulletin **544**. (in press)

Wu, R.S., and Aki, K., 1985, The fractal nature of inhomogeneities in the lithosphere evidenced from seismic wave scattering: *Pure and Applied Geophysics*, **123**, 805–813.

Yamazaki, F., and Shinozuka, M., 1988, Digital generation of non-Gaussian stochastic fields: *J. Eng. Mech., ASCE*, **116**, 268-287.

APPENDIX

Finding an input PSDF of Gaussian random medium

Non-linear mapping with equation (10) yields an autocorrelation function (ACF) and power spectral density (PSDF) for the bimodal random medium which are inconsistent with the required values. Yamazaki and Shinozuka (1988) proposed an iterative method for generating a non-Gaussian random field to satisfy the desired PSDF, S_d, by updating the input PSDF of a Gaussian random medium. We use their method to obtain the input PSDF of a Gaussian random medium, S_g, as shown in the flow chart in Figure 9. Given the PSDF of a Gaussian random medium at the ith iteration, $S_g^{(i)}(\mathbf{K})$, an initial bimodal random medium is generated as described in the Modelling Methodlogy section. Then, the PSDF of the Gaussian random medium at the $(i+1)$th iteration is defined as

$$S_g^{(i+1)}(\mathbf{K}) = \frac{S_g^{(i)}(\mathbf{K})}{S_b^{(i)}(\mathbf{K})} S_d(\mathbf{K}) , \qquad (13)$$

where $S_b^{(i)}(\mathbf{K})$ is the PSDF of the bimodal random medium at the ith iteration. The initial PSDF of Gaussian random medium is set to be equal to the desired PSDF. When $S_b^{(i)}(\mathbf{K})$ converges to $S_d(\mathbf{K})$, $S_g(\mathbf{K})$ is given by $S_g^{(i)}$. The final bimodal random medium is then generated using this $S_g(\mathbf{K})$ function as input.

Figures 10 and 11 show an example. Before the iteration begins, the PSDF of the bimodal random media is different from the desired PSDF (Figure 10) especially at high frequencies. After 9 iterations, the PSDF of the bimodal random medium matches fairly well at both low and high frequencies (Figure11).

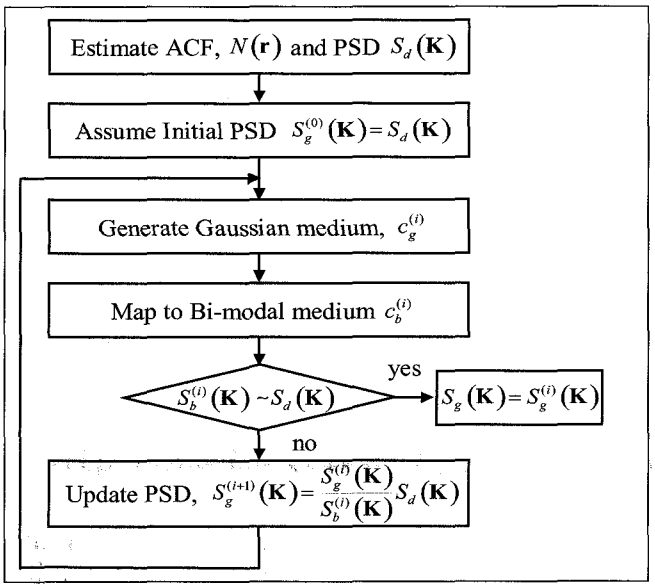

Fig. 9. Flow chart for the procedure for generating S_g.

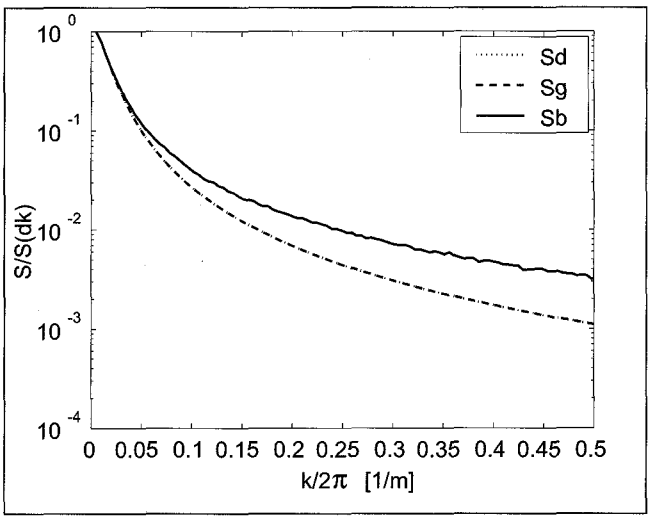

Fig. 10. Gaussian and bimodal PSDFs before starting iteration 1. The horizontal axis is the wave number $k/2\pi$, and the vertical axis is PSDF normalized with its value at $k = dk$. The dotted line denotes a desired PSDF (S_d), the dashed line is a PSDF for Gaussian random media ($S_g^{(0)}$), and the solid line is a PSDF for a bimodal random medium, $S_b^{(0)}$. $S_g^{(0)}$ and S_d coincide, by definition. $S_b^{(0)}$ does not agree with S_d.

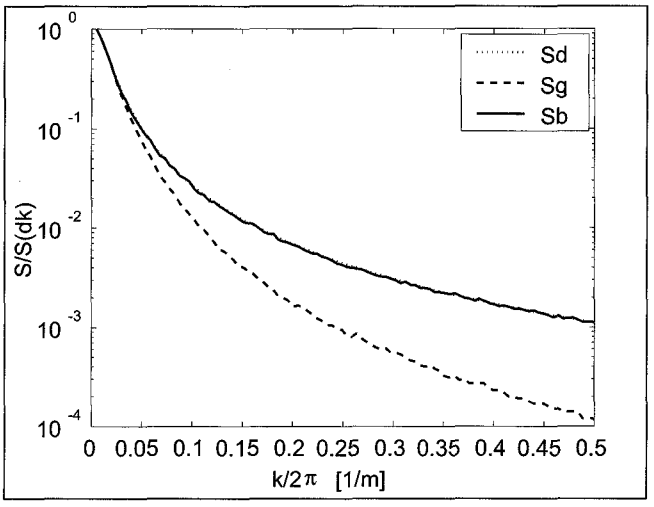

Fig. 11. PSDFs after 9 iterations. $S_b^{(9)}$ is almost coincident with S_d, but $S_g^{(9)}$ is quite different from from S_d.

バイモーダル分布型ランダム不均質媒質によるメタンハイドレート層モデル化

亀井理映[1]・羽藤正実[2]・松岡俊文[1]

要　旨：　メタンハイドレートは将来のエネルギー資源として期待されており、その資源量推定および生産にあたっては、正確なハイドレート層モデル化が不可欠である。坑井での検層情報から、ハイドレート層は短周期の不均質性を持っていると考えられ、こうした短波長不均質が地震波の散乱を引き起こすことが知られている。本論文では、ハイドレート層を、検層情報に基づきランダム不均質媒質としてモデル化する手法を開発し、数値シミュレーションにより、不均質性に起因する散乱が地震探査記録に与える影響を考察した。

ハイドレート層の不均質性は、P 波速度検層より von Karman 型の自己相関関数により特徴づけられる。また、確率密度関数(ヒストグラム)は数 100m/s の隔たりのある 2 箇所にピークを持ち、異なる平均値を持つ正規分布の重ね合わせと見なすことのできるバイモーダル分布により表現可能である。バイモーダル分布に従うランダム不均質媒質は、パワースペクトルを基に作成される正規分布に従う通常のランダム不均質媒質を変換することで求められる。また、楕円型自己相関関数を用いることで、異方性を持つ媒質も生成可能である。この手法を用いて生成した P 波速度ログは、実際の P 波速度ログに見られる特徴を再現可能であり、手法の妥当性が示された。続いて、バイモーダル速度分布をハイドレート層に適用し、差分法を用いた弾性波動シミュレーションにより、合成反射法地震探査データおよび合成坑井間地震探査データを作成し、検討を行った。その結果、実際のハイドレート地震探査でしばしば見られる BSR の震源周波数依存性を再現可能であり、また、坑井間地震探査データで見られる強い減衰も再現された。これらの検討の結果、ハイドレート層モデル化にあたっては、バイモーダル分布に従うランダム不均質性の考慮が不可欠と結論づけられる。

바이모달 분포형태 랜덤 불균질 매질에 의한 메탄하이드레이트층 모델화

Rie Kame[1]・Masami Hato[2]・Toshifumi Matsuoka[1]

요　약：　이 연구에서는 메탄 하이드레이트 부존 지역의 속도 분포를 구하기 위해서 무작위 불균질 모델을 개발하였다. P 파 물리검층 자료는 von Karman 유형의 자기상관함수와 비가우스 확률 분포를 가진다. 속도 분포는 수백 m/s 의 차이가 나는 두 개의 정점(peak)들을 갖는다. 이중모드 속도 분포를 가진 무작위 불균질 매질의 모델은 normal spectral-based generation 방법에 의해 만들어진, 가우스 속도 분포를 갖는 매질의 사상을 통해 만들어졌다. 또한 타원 자기상관 함수를 이용하여 무작위 매질에 자기상관 길이의 이방성을 첨가하였다. 유사 P 파 속도 검층기록은 현장자료의 특징을 잘 구현해냈다.

이 모델을 두 개의 탄성파 전파 수치 모형에 적용하였다. 두 개의 다른 주파수 대역의 송신신호들에 의해 만들어진 합성 반사 단면도들을 통해 이중모드 분포를 가진 무작위 모델의 속도 변화가 파의 산란에 영향을 줌으로써 BSR 의 주파수 의존성의 원인이 됨을 알 수 있다. 합성 시추공간 단면도는 현장자료에서 보여지는 심한 감쇠가 산란에 의한 부가적인 진폭 감쇠에 의한 것임을 보여주고 있다.

결론적으로 이중모드 분포를 가진 무작위 불균질성은 하이드레이트 부존층 모델링의 핵심이고, 이를 통해 하이드레이트 부존 지역의 탄성파 단면도들에서 관찰되는 주파수 의존성과 산란현상에 대해 설명할 수 있다.

1 京都大学大学院工学研究科　社会基盤工学専攻
〒606-8501　京都府京都市左京区吉田本町
2 (株)地球科学総合研究所

1교토대학대학원공학연구과　사회기반공학전공
2 (주)지구과학종합연구소